^{20}Ne nuclear moments from ^{20}Ne(131 MeV) + ^{208}Pb scattering

E. E. Gross, T. P. Cleary, J. L. C. Ford, D. C. Hensley, and K. S. Toth
Oak Ridge National Laboratory, Oak Ridge, Tennessee 37830
(Received 12 December 1977)

We have measured differential cross sections for elastic and inelastic scattering of ^{20}Ne + ^{208}Pb at a lab energy of 131 MeV. Inelastic data for exciting the ^{20}Ne 2^+ (1.63 MeV) state and a group of states near 4.2 MeV are presented. The data are analyzed by a rotational-model coupled-channels calculation including the ground state, 2^+, and 4^+ states of ^{20}Ne. We obtain the values: transition moment $B(E2\uparrow) = (0.0330 \pm 0.0015)\ e^2\,b^2$, intrinsic hexadecapole moment $Q_{40} = (0.022 \pm 0.003)\ e^2\,b^2$, and static quadrupole moment for the ^{20}Ne 2^+ state $Q_2 = (-0.27 \pm 0.03)\ e$ b. The result for Q_2 emphasizes a discrepancy with the rotational model and with various shell model calculations.

[NUCLEAR REACTIONS ^{208}Pb(^{20}Ne, ^{20}Ne), ^{208}Pb(^{20}Ne, ^{20}Ne'), $E = 131$ MeV, measured $\sigma(\theta)$; deduced optical potential, quadrupole deformation parameter, hexadecapole deformation parameter, and static quadrupole moment of ^{20}Ne by a coupled-channels analysis. Enriched target.]

I. INTRODUCTION

Heavy-ion inelastic scattering at energies below the Coulomb barrier (i.e., Coulomb excitation) has long been a useful technique for obtaining information on the shapes of nuclear charge distributions. Since nuclear moments are sensitive to the details of the nuclear wave function, these data have been an important testing ground for the collective model and the nuclear shell model theories. Analyses of heavy-ion inelastic scattering experiments have also stimulated the development of nuclear reaction theories, especially the quantum-mechanical coupled-channels (CC) theory. Extending this approach to energies above the Coulomb barrier has usually been avoided because of the nonanalytic nature of the ion-ion nuclear potential. However, in a recent study[1] of 70 MeV ^{12}C inelastic scattering from the even Nd isotopes, it was shown that this obstacle could be overcome by a careful CC analysis of the data. In addition, it was found that above-the-barrier inelastic scattering with heavy ions involved a strong nuclear reorientation effect for 2^+ rotational states.[1-4]

The present work is an attempt to apply this technique to the nuclear moments of ^{20}Ne about which there are experimental disagreements regarding $B(E2\uparrow)$ values[5-8] and for which the available experimental information on the quadrupole moment of ^{20}Ne in its 2^+ state[5,8,9] suggests a problem in understanding this quantity within the shell model.[10-14] To this end, we measured the elastic scattering angular distribution of 131 MeV ^{20}Ne from a ^{208}Pb target as well as the differential cross section for exciting ^{20}Ne to its lowest 2^+ state (1.63 MeV). We then analyzed the data with the CC rotational-model formalism and obtained the quadrupole charge deformation parameter, β_2^C, the hexadecapole charge deformation parameter, β_4^C, and the static quadrupole moment of ^{20}Ne in its 2^+ state, Q_2. Finally, we compare our results to other determinations.

II. EXPERIMENTAL DETAILS AND RESULTS

The 131.0 ± 0.1 MeV ^{20}Ne^{6+} beam was provided by the Oak Ridge isochronous cyclotron. The target consisted of 100 μg/cm^2 ^{208}Pb evaporated onto a 50 μg/cm^2 carbon foil, and the mean energy in the target was estimated to be 130.9 ± 0.2 MeV. Most of the data were obtained with a position-sensitive solid-state detector (PSD) located on a moveable arm within a 76 cm diameter scattering chamber. A 15-element slit before the PSD defined 0.5° angular apertures centered at 1° intervals. The elastic scattering angular distribution was measured with this device over the angular range of $14° \leq \theta_{c.m.} \leq 87°$ by overlapping neighboring angular ranges of the slit system by at least two angles. These data were normalized by assuming the elastic scattering cross section to have its Rutherford value for angles less than 20° c.m. The elastic scattering data as a ratio to Rutherford scattering are shown in Fig. 1 for the angles greater than 20° c.m. Further experimental details as well as the method of data acquisition and data reduction may be found in Ref. 15.

The same device provided the ^{20}Ne 2^+ state (1.63 MeV) data between $\theta_{c.m.} = 33°$ and $\theta_{c.m.} = 68°$ shown as open circles in Figs. 2–4. Error bars are mainly statistical but also contain a contribution from unfolding the 2^+ yield from the elastic tail. The val-

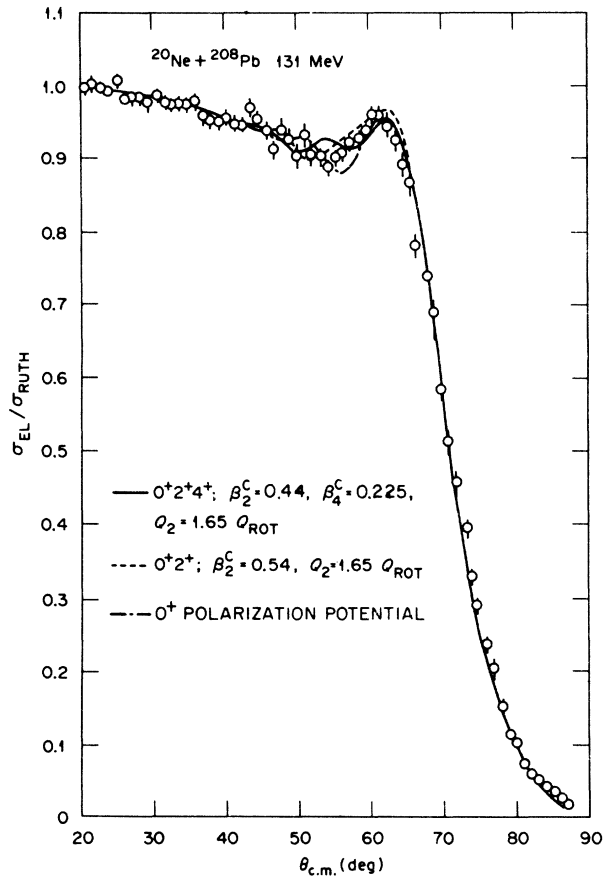

FIG. 1. ^{20}Ne (131 MeV) + ^{208}Pb elastic scattering relative to Rutherford scattering. The dotted curve is our best $0^+ \longleftrightarrow 2^+$ CC calculation. The solid curve is our best $0^+ \longleftrightarrow 2^+ \longleftrightarrow 4^+$ CC calculation involving all the transitions in Fig. 6. The dot-dash curve is an optical model fit where Coulomb excitation is approximated by an additional long-range absorption (Ref. 20). All three calculations use the same $B(E2\uparrow) = 0.033e^2b^2$ to account for excitation of the ^{20}Ne 2^+ state.

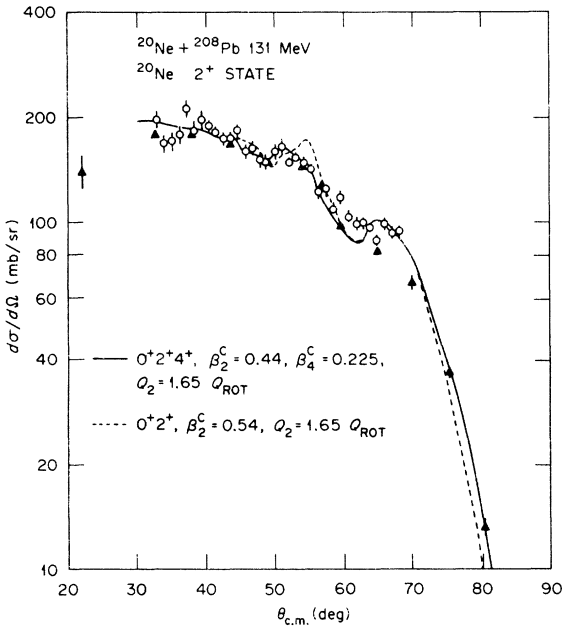

FIG. 2. Differential cross section for exciting the ^{20}Ne 2^+ state (1.63 MeV) by 131 MeV ^{20}Ne scattering from ^{208}Pb. The open circles are solid state detector measurements and the closed triangles are spectrograph measurements. The dotted curve is our best $0^+ \longleftrightarrow 2^+$ calculation corresponding to the elastic scattering fit in Fig. 1 and the solid curve is our best $0^+ \longleftrightarrow 2^+ \longleftrightarrow 4^+$ fit. The calculations are unreliable for $\theta_{c.m.} \lesssim 30°$.

ues of the absolute cross sections depend on the above-mentioned normalization of the elastic cross section and are believed to be reliable to 3%. The 2^+ data shown as solid triangles in Figs. 2–4 as well as the data on a group of states near 4.2 MeV shown in Fig. 5 were obtained using a spectrograph with a position-sensitive gas proportional detector at the focal plane. The overall resolution obtained in the spectrograph was 0.20 MeV—not enough to resolve the ^{20}Ne 4^+ state (4.25 MeV) from a ^{208}Pb 2^+ state (4.09 MeV) and a ^{208}Pb 4^+ state (4.32 MeV). Excitation of ^{208}Pb 3^- (2.63 MeV) was also observed with an average cross section of 6 mb/sr. Further details concerning the spectrograph methods used here may be found in Ref. 1.

III. ANALYSIS

The analysis of our ^{20}Ne data was carried out within the framework of the collective rotational model incorporated into the CC method.[16] The computer program ECIS,[17] which was used for the analysis, is formulated in terms of a radius vector directed from the center of the target to the center of the projectile. The "nuclear surface" described by this vector is the surface generated by the center of one nucleus, which we will assume to be spherical, as it is rolled over the surface of a second deformed nucleus. The charge surface of the deformed nucleus is assumed to be described by the radius parameter

$$R_2^C(\theta) = r^C A_2^{1/3}\left[1 + \beta_2^C Y_{20}(\theta) + \beta_4^C Y(\theta) + \dots\right], \quad (1)$$

whereas the "nuclear surface" is assumed to be described by

$$R_2^N(\theta) = r^N(A_1^{1/3} + A_2^{1/3})\left[1 + \beta_2^N Y_{20}(\theta) + \beta_4^N Y_{40}(\theta) + \dots\right]. \quad (2)$$

On the basis of the rolling model, Hendrie[18] has

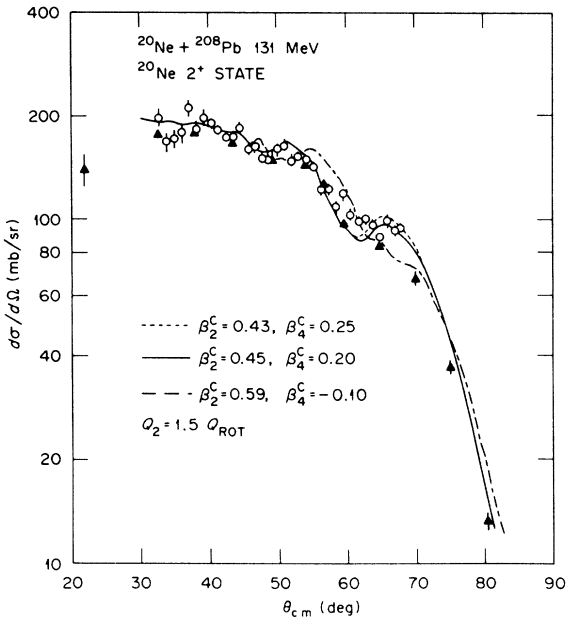

FIG. 3. Three $0^+ \longleftrightarrow 2^+ \longleftrightarrow 4^+$ calculations with different values of β_4^C are compared by their 2^+ cross section predictions. All calculations have the same $B(E2\uparrow)$ value, $0.033e^2b^2$ and the same value for $Q_2 = 1.5|Q_{Rot}|$ (not the best fit value). The values of β_2^C are then fixed by Eq. (3) in the text. The level of the 2^+ cross section near $\theta_{c.m.} = 65°$ then picks out the magnitude of β_4^C and the shape of the 2^+ cross section between 50° and 70° determines the sign of β_4. The calculations are unreliable for $\theta_{c.m.} \lesssim 30°$.

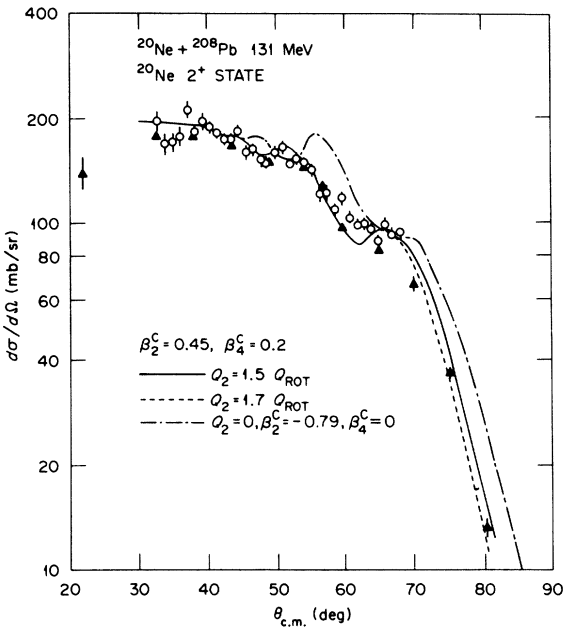

FIG. 4. Three $0^+ \longleftrightarrow 2^+ \longleftrightarrow 4^+$ calculations are compared for sensitivity to the reorientation effect on the predicted 2^+ cross section. All calculations have the same $B(E2\uparrow)$ value and therefore they have the same magnitude for the forward angle 2^+ cross section. For a given shape (i.e., prolate or oblate), the magnitude of Q_2 affects the magnitude of the 2^+ cross section for angles greater than 70° c.m. Sensitivity to the sign of β_2^C may be judged by comparing the dot-dash curve to either the solid or dashed curves. The calculations are unreliable for angles less than 30°.

shown how to relate deformations measured on the "nuclear surface" (β_2^N, β_4^N, etc.) to deformations of the target surface (β_2^C, β_4^C, etc.). Although Hendrie[18] provides this relation to second order in β, it is an easy matter to extend the derivation to higher orders. The procedure should be valid for strongly absorbed projectiles and appears to provide a satisfactory description for 50 MeV α scattering from rare earth nuclei[18,19] and for 70 MeV ^{12}C scattering from Nd nuclei.[1,3] Neither of these experiments depends on the higher order terms of the rolling model as much as does the present work with the nucleus ^{20}Ne which appears to be a very deformed object with $\beta_2^C \approx +0.45$ and $\beta_4^C \approx +0.2$.

Most of the CC calculations reported here employed the transitions shown in Fig. 6 and included all orders in the reorientation transition. Couplings of states in ^{208}Pb with states in ^{20}Ne are assumed to be unimportant and are not included. The effects of exciting states in ^{208}Pb, as well as all other absorption processes, are presumably accounted for by adjustment of the optical potential (primarily the imaginary part) to give a simultaneous fit to elastic scattering and inelastic excitation of ^{20}Ne to its 2^+ state. In addition to the six parameters of the optical potential (V, r_0, a_0 for the real potential and W, r', a' for the absorptive volume potential), there are three nuclear moment parameters, β_2^C, β_4^C, and Q_2 describing ^{20}Ne. Although the $4^+ \rightarrow 2^+$ transition strength appears to be about 15% lower than the rotational-model expectation,[6] we use the rotational-model value in the results reported here. One calculation with the $2^+ \longleftrightarrow 4^+$ matrix elements reduced by 15% made a negligible effect on the calculated 0^+ and 2^+ cross sections but made a noticeable effect on the predicted 4^+ cross section. As explained above, the nuclear deformations β_2^N and β_4^N are not independent parameters but are derived from β_2^C and β_4^C using the rolling model.[18] The rolling model applied to ^{20}Ne + ^{208}Pb also generates a small $\beta_6^N \approx -0.02$ term which is included in our calculations. Since heavy-ion scattering at energies slightly above the Coulomb barrier is not sensitive to the nuclear interior, the optical model well depths and radius parameters are related by the usual ambiguities, and there are actually only four independent optical model parameters. These optical model parame-

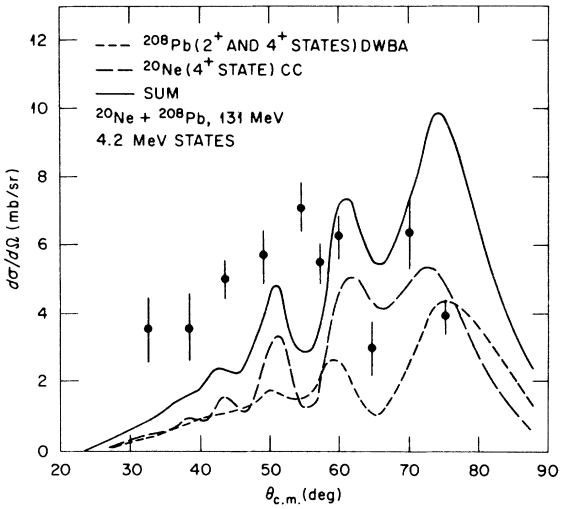

FIG. 5. Differential cross section for exciting a group of states near 4.25 MeV which include the ^{20}Ne 4^+ (4.25 MeV), ^{208}Pb 2^+ (4.09 MeV), and ^{208}Pb 4^+ (4.3 MeV) states by 131 MeV ^{20}Ne scattering from ^{208}Pb. The short dashed curve is a DWBA estimate of the contribution from the two ^{208}Pb states and the long dashed curve is the ^{20}Ne 4^+ cross section prediction resulting from our best $0^+ \longleftrightarrow 2^+ \longleftrightarrow 4^+$ CC calculation. The solid curve is the sum of the dashed curves.

ters are most sensitive to the elastic scattering angular distribution, whereas the quadrupole deformation, β_2^C, is most sensitive to the magnitude of the forward angle 2^+ cross section. The quadrupole moment of the 2^+ state, Q_2, is most sensitive to the 2^+ cross section at back angles[1-3] and, as we will see below, the hexadecapole moment, β_4^C,

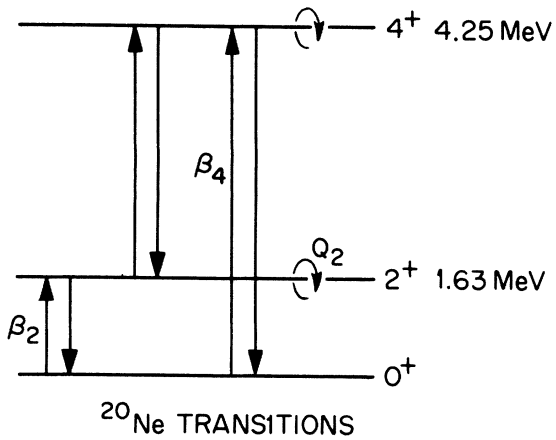

FIG. 6. Rotational-model transitions included in the $0^+ \longleftrightarrow 2^+ \longleftrightarrow 4^+$ calculations. In a DWBA calculation, the strength of the $0^+ \rightarrow 2^+$ transition is proportional to β_2^2 and the strength of the $0^+ \rightarrow 4^+$ transition is proportional to β_4^2. In the rotational-model CC calculations all transitions depend on β_2 and β_4. In our calculations β_2^C, β_4^C, and Q_2 are treated as adjustable parameters.

is most sensitive to the 2^+ cross section near the grazing angle. It is this partial separation of sensitivities together with high quality data covering a large angular range that makes it possible to determine a fairly unique set of parameters.

Initial optical model parameters were obtained by fitting the elastic scattering and 2^+ data with only the $0^+ \longleftrightarrow 2^+$ coupling included. Most calculations employed 300 partial waves and the radial integrals were carried out to 50 fm in 0.05 fm steps. This number of partial waves is adequate for representation of the 2^+ cross section for angles greater than about 30°. We began with a potential found to fit ^{20}Ne+^{208}Pb elastic scattering at 160 MeV, [15] $\beta_2^C = +0.54$ and $Q_2 = 1.65\,|Q_{\rm Rot}|$. The value of β_2^C accounts for the magnitude of our 2^+ cross section data for $\theta_{c.m.} \lesssim 50°$ and implies a value of $B(E2\uparrow) = 0.032e^2\,\mathrm{b}^2$ from the relation

$$[B(E2\uparrow)]^{1/2} = \int \rho(r,\theta) r^2 Y_{20}(\theta) d\tau \ , \qquad (3)$$

where we assume a homogeneous charge distribution out to the radius $R_2^C(\theta)$ of Eq. (1) and zero charge for $r > R_2^C(\theta)$. The value $Q_2 = 1.65\,|Q_{\rm Rot}|$ was suggested from previous Coulomb reorientation measurements[5,8,9] and is near the value required to fit our large angle 2^+ data. In Fig. 1 we show as a dashed curve the best $0^+ \longleftrightarrow 2^+$ fit to elastic scattering with these nuclear moment parameters and with the optical potential $V = 21.5$ MeV, $r_0 = 1.34$ fm, $a_0 = 0.49$ fm, $W = 7.0$ MeV, $r' = 1.43$ fm, and $a' = 0.3$ fm. The corresponding fit to the 2^+ data is shown as the dashed curve in Fig. 2. Also shown in Fig. 1 is a fit to elastic scattering using the "polarization potential" method[20] (dot-dash curve). In this method, Coulomb excitation to the 2^+ state is accounted for by an additional long-range absorptive potential. Finally, the best $0^+ \longleftrightarrow 2^+ \longleftrightarrow 4^+$ calculation is shown as the solid curves in Figs. 1 and 2. In this calculation, the optical potential is identical to that for the $0^+ \longleftrightarrow 2^+$ calculation except that W has been reduced from 7.0 to 5.0 MeV to account for effects of including the 4^+ state in the CC calculation. All three fits to the elastic scattering are quite satisfactory since they have χ^2 values per point of about 1.1 to 1.3. The elastic scattering as a ratio-to-Rutherford scattering (Fig. 1) has been plotted on a linear scale to emphasize the behavior before the exponential falloff. Nevertheless, the slight disagreement near 55° between the best calculation and the data is an indication that there is still something missing from the calculation.

Comparison of the 2^+ fits in Fig. 2 reveals that the $0^+ \longleftrightarrow 2^+ \longleftrightarrow 4^+$ calculation represents a significant improvement over the $0^+ \longleftrightarrow 2^+$ calculation for $50° \lesssim \theta_{c.m.} \lesssim 60°$. It is curious that the magnitude

of the 2^+ cross section in the range $60° \leq \theta_{c.m.} \leq 70°$ plays a central role in fixing the magnitude of the hexadecapole deformation parameter, β_4^C. This is illustrated in Fig. 3 where calculations for three values of β_4^C are compared. The three calculations use the same $B(E2\uparrow)$ and the values of β_2^C are then determined by Eq. (3). The magnitude of the 2^+ cross section near 65° then favors the value $\beta_4^C = +0.225$. The shape of the 2^+ data between 50° and 70° rules out the negative sign for β_4 (dot-dash curve in Fig. 3). Again, the slight deviation of the best 2^+ calculation from the data near 63° is a possible indication of something lacking in the calculation. Sensitivity to the value of Q_2 is illustrated in Fig. 4. The three calculations shown are for the same $B(E2\uparrow)$ value but differing values of Q_2. The dot-dash curve is a calculation for an oblate shape ($\beta_2^C = -0.78$, $\beta_4^C = 0$) with $Q_2 = 0$. For values of $|Q_2| > 0$, the oblate calculation predicts even larger magnitude yields for $\theta_{c.m.} > 70°$ and an oblate shape can be ruled out.

Presumably, data for the ^{20}Ne 4^+ state would be most helpful in establishing the value of β_4^C, but this level could not be resolved from levels populated in ^{208}Pb. The data for levels near 4.2 MeV are displayed in Fig. 5 along with our calculated cross section for the 4.25 MeV state in ^{20}Ne (dashed curve). The contributions from the 2^+ (4.09 MeV) and 4^+ (4.32 MeV) levels in ^{208}Pb were estimated (dotted curve) with distorted-wave Born approximation (DWBA) calculations using deformation parameters reported previously[21] and the optical potential $V = 22.5$ MeV, $r_0 = 1.33$ fm, $a_0 = 0.44$ fm, $W = 15.2$ MeV, $r' = 1.29$ fm, $a' = 0.67$ fm, $r^C = 1.25$ fm. The solid curve in Fig. 5 is the sum of the dotted and dashed curves and is to be compared with the data. Owing to the uncertainties involved in estimating the contributions from the ^{208}Pb levels, all that one can say is that the ^{20}Ne 4^+ cross section has about the correct magnitude and angular behavior.

A calculation including the ^{20}Ne 6^+ (8.79 MeV) state[22] was performed with 200 partial waves to assess the effects of triple $E2$ excitation. Inclusion of the 6^+ state, with $\beta_6^C = 0$, increased the 4^+ cross section peak near 75° by about 30% but had no noticeable effect on the predicted 0^+ and 2^+ cross sections.

IV. DISCUSSION

From a least squares fit to the 2^+ cross section in the Coulomb dominated region ($32° \leq \theta_{c.m.} \leq 51°$), we obtain $B(E2\uparrow) = (0.0330 \pm 0.0015) e^2\,b^2$ where the error includes a contribution from the uncertainty in the absolute cross section. As described above, we obtain $\beta_4^C = +0.225 \pm 0.030$ from a fit to the 2^+

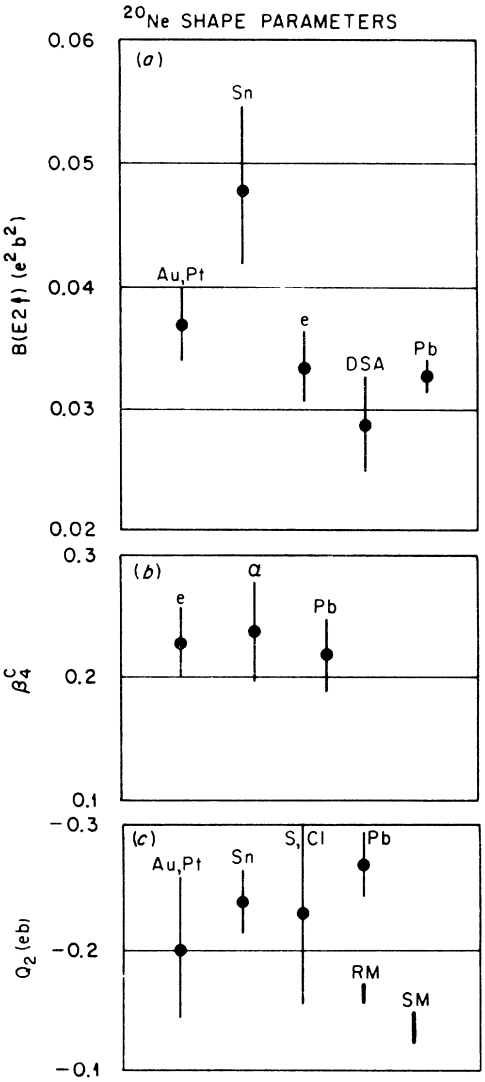

FIG. 7. Comparison of ^{20}Ne shape parameters obtained by different methods. (a) compares the present $B(E2\uparrow)$ measurement (Pb) with (1) Coulomb excitation from Au and Pt targets (Ref. 8), (2) Coulomb excitation from a Sn target (Ref. 5), (3) electron (e) scattering (Ref. 7), and (4) with a Döppler shift attenuation (DSA) measurement of the ^{20}Ne 2^+ state lifetime. (b) compares our Pb measurement of the hexadecapole deformation parameter, β_4^C, with that from electron scattering (Ref. 7) and with the value obtained from 104 MeV α-particle scattering (Ref. 23). The charge radius was taken to be $R_C = 1.25(20)^{1/3}$ fm. (c) compares the present (Pb) determination of the spectroscopic quadrupole moment, Q_2, with (1) Coulomb reorientation from Au and Pt targets (Ref. 8), (2) Coulomb reorientation from a Sn target (Ref. 5), and (3) Coulomb reorientation using S and Cl beams (Ref. 9). The (Pb) measurement is properly characterized as a nuclear reorientation measurement. The bar labeled RM is calculated from the rotational model [Eq. (4)] using the average $B(E2\uparrow)$ of (a). The bar labeled SM represents the results from a variety of shell model calculations (Refs. 10–14).

TABLE I. Experimental results for multipole moments and deformation parameters for ^{20}Ne.

"Projectile" or reaction	$B(E2\uparrow)$ (e^2b^2)	Q_{40} (e^2b^2)	Q_2 (eb)	β_2^C	β_4^C	Reference
^{12}C(^{12}C, $\alpha\gamma$)^{20}Ne	0.029 ±0.003	...	...	...	...	6
^{120}Sn	0.048 ±0.007	...	−0.24 ±0.03	...	...	5
^{32}S, ^{34}S, ^{37}Cl	...	...	−0.23 ±0.08	...	...	9
Au, Pt	0.037 ±0.003	...	−0.20 ±0.06	...	...	8
e	0.0335 [a] ±0.0035	0.021 [b] ±0.002	...	+0.40 [c] ±0.01	+0.23 [c] ±0.03	7
α	0.043 [e] ±0.005	0.026 [e] ±0.004	...	+0.48 [d] ±0.02	+0.24 [d] ±0.04	23
^{208}Pb	0.0330 ±0.0015	0.022 ±0.003	−0.27 ±0.03	+0.44 ±0.01	+0.225 ±0.03	This experiment

[a] Calculated from the reported (Ref. 7) $Q_{20}=(58\pm3)e\,\mathrm{fm}^2$ by the relation $Q_{20}=(16\pi/5)^{1/2}\times[B(E2\uparrow)]^{1/2}$.

[b] Calculated from the reported (Ref. 7) $H_0=(249\pm27)e^2\,\mathrm{fm}^4$ by the relation $Q_{40}=(9/4\pi)^{1/2}H_0$.

[c] Calculated from simultaneous solution of Eqs. (4) and (5) for β_2^C and β_4^C.

[d] Calculated from the rolling model (Ref. 18). With a nuclear radius parameter (Ref. 23) of 1.37 fm, rolling a spherical α particle over a deformed ^{20}Ne($\beta_2^C=+0.4$ and $\beta_4^C=+0.2$) would generate $\beta_2^N=+0.35$, $\beta_4^N=+0.11$ on the "nuclear surface." These nuclear values are the ones reported in Ref. 23.

[e] Calculated from Eqs. (4) and (5) from the values of β_2^C and β_4^C in columns 5 and 6.

cross section near 65° c.m. and $Q_2=(-1.65\pm0.15)\,|Q_2|_{\mathrm{Rot}}$ from a fit to the 2$^+$ cross section for $\theta_{\mathrm{c.m.}}>70°$. These errors are subjective judgments as to the limits of an acceptable fit. We then determine β_2^C from β_4^C, $B(E2\uparrow)$, and Eq. (3) to be $\beta_2^C=0.44\pm0.01$. The rotational model relates the spectroscopic quadrupole moment, $|Q_2|_{\mathrm{Rot}}$ for the $K=0$ band to the $B(E2\uparrow)$ by

$$|Q_2|_{\mathrm{Rot}}=\left(\frac{16\pi}{5}\right)^{1/2}\times\frac{2}{7}\times[B(E2\uparrow)]^{1/2}. \tag{4}$$

We then obtain a spectroscopic quadrupole moment for ^{20}Ne which is $Q_2=(-0.27\pm0.02)e$b. Contributions to Q_2 from giant dipole transitions are expected[9] to be less than $0.01e$ b. Our values for the ^{20}Ne shape parameters are compared to other determinations in Fig. 7 and in Table I. With the exception of the value obtained from the Coulomb excitation of a Sn target,[5] the various $B(E2\uparrow)$ measurements [Fig. 7(a)] agree. These measurements include Coulomb excitation from Au and Pt targets,[8] high energy electron scattering,[7] and a life-time measurement by the Döppler-shift attenuation method.[6] Hexadecapole deformation parameters, shown in Fig. 7(b), as well as intrinsic hexadecapole moments, column 4 of Table I, are also in agreement. Our value $Q_{40}=(0.022\pm0.003)e^2b^2$ was calculated from the above β_2^C and β_4^C values and the relation

$$Q_{40}=\left(\frac{16\pi}{9}\right)^{1/2}\int\rho(r,\theta)r^4Y_{40}(\theta)d\tau. \tag{5}$$

The electron scattering value[7] for β_4^C has been slightly adjusted to account for the second order approximation used[7] in evaluating the integral in Eq. (3) as well as in evaluating the corresponding integral for the intrinsic hexadecapole moment [Eq. (5)]. The β_4^C value obtained from 104 MeV inelastic α particle scattering[23] has been adjusted by the rolling model procedure[18] to represent a deformation on the target surface. This is a rather large adjustment from the reported value[23] of $\beta_4^N=+0.11\pm0.01$. However, a folding model analysis[24] of the α-scattering experiment[23] also yielded β_4^C values (+0.27 to +0.29) similar to the value shown in Fig. 7(b). The determination of the hexadecapole deformation parameter from the analysis of 104 MeV α-particle scattering[23] or from 250 MeV electron scattering[7] appears to depend critically on the observed ^{20}Ne 4$^+$ cross section. It is therefore worth emphasizing that the present measurement,

using, heavy-ion inelastic scattering at an energy slightly over the Coulomb barrier, arrives at a similar hexadecapole deformation parameter by an analysis of only the elastic scattering and 2^+ cross sections. Also note that, of all the experiments summarized in Table I, heavy-ion inelastic scattering above the Coulomb barrier is the only technique which provides simultaneous values for $B(E2\uparrow)$, Q_{40}, and Q_2. Results from 30 MeV proton inelastic scattering[25] from ^{20}Ne have not been included in Fig. 7 or in Table I because the partial transparency of 30 MeV protons to nuclear matter[26] makes the rolling model inapplicable.

In Fig. 7(c), the present determination of Q_2 for ^{20}Ne is compared to measurements[5,8,9] by the Coulomb reorientation method. Our value is primarily a nuclear matter quadrupole moment in contrast to the charge quadrupole moment determined by Coulomb reorientation. All the results are in agreement within error limits, but the new determination emphasizes the theoretical problem of understanding the large magnitude of the static quadrupole moment of ^{20}Ne. The rotational-model prediction for $Q_{2_{\mathrm{Rot}}}$ [Eq. (4)] shown in Fig. 7(c) is based on the average $B(E2\uparrow)$ of Fig. 7(a). Although the shell model predictions come from calculations[10-14] which employ a variety of wave functions, nucleon-nucleon interactions, and configuration spaces, they all predict very similar quadrupole moments. The shell model predictions as well as the rotational-model expectation appear to be ~50% lower than experimental values.

It is a pleasure to acknowledge several helpful conversations with F. T. Baker. We are also indebted to him for providing us with his computer program to calculate intrinsic multipole moments and rolling model deformation parameters. To G. R. Satchler we owe the results of the calculation of elastic scattering by the polarization potential method. This research was supported by Union Carbide Corporation under contract with the U. S. E. R. D. A.

[1]D. L. Hillis, E. E. Gross, D. C. Hensley, C. R. Bingham, F. T. Baker, and A. Scott, Phys. Rev. C 16, 1467 (1977).
[2]F. Videbaek, P. R. Christensen, O. Hansen, and K. Ulbak, Nucl. Phys. A256, 301 (1976).
[3]D. L. Hillis, E. E. Gross, D. C. Hensley, L. D. Rickertsen, C. R. Bingham, A. Scott, and F. T. Baker, Phys. Rev. Lett. 36, 304 (1976).
[4]J. X. Saladin, I. Y. Lee, R. C. Haight, and D. Vitous, Phys. Rev. C 14, 992 (1976).
[5]K. Nakai, F. S. Stephens, and R. M. Diamond, Nucl. Phys. A150, 114 (1970).
[6]O. Häusser, T. K. Alexander, A. B. McDonald, G. T. Ewan, and A. E. Litherland, Nucl. Phys. A168, 17 (1971).
[7]Y. Horikawa, Y. Torizuka, A. Nakada, S. Mitsunobu, Y. Kojima, and M. Kimura, Phys. Lett. 36B, 9 (1971).
[8]D. K. Olsen, W. R. Phillips, and A. R. Barnett, Phys. Lett. 39B, 201 (1972).
[9]D. Schwalm, A. Bamberger, P. G. Bizzeti, B. Povh, G. A. P. Engelbertink, J. W. Olness, and E. K. Warburton, Nucl. Phys. A192, 449 (1972).
[10]M. R. Gunye, Phys. Lett. 37B, 125 (1971).
[11]A. Arima, M. Sakakura, and T. Sebe, Nucl. Phys. A170, 273 (1971).
[12]B. H. Wildenthal, J. B. McGrory, and P. M. Glaudemans, Phys. Rev. Lett. 26, 96 (1971).
[13]J. Zofka and G. Ribka, Nucl. Phys. A168, 65 (1971).
[14]S. Krewald, K. W. Schmid, A. Faessler, and J. B. McGrory, Nucl. Phys. A228, 524 (1974).
[15]J. B. Ball, C. B. Fulmer, E. E. Gross, M. L. Halbert, D. C. Hensley, C. A. Ludemann, M. J. Saltmarsh, and G. R. Satchler, Nucl. Phys. A252, 208 (1975).
[16]T. Tamura, Rev. Mod. Phys. 37, 679 (1965).
[17]J. Raynal, Private communication.
[18]D. L. Hendrie, Phys. Rev. Lett. 31, 478 (1973).
[19]D. L. Hendrie, N. K. Glendenning, B. G. Harvey, O. N. Jarvis, H. H. Duhm, J. Saudinos, and J. Mahoney, Phys. Lett. 26B, 127 (1968).
[20]W. G. Love, T. Terasawa, and G. R. Satchler, Phys. Rev. Lett. 39, 6 (1977).
[21]J. L. C. Ford, K. S. Toth, D. C. Hensley, R. M. Gaedke, P. J. Riley, and S. T. Thornton, Phys. Rev. C 8, 1912 (1973).
[22]J. A. Kuehner and J. D. Pearson, Can. J. Phys. 42, 477 (1964).
[23]H. Rebel, G. W. Schweimer, G. Schatz, J. Specht, R. Löhken, G. Hauser, D. Habs, and H. Klewe-Nebenius, Nucl. Phys. A182, 145 (1972).
[24]H. Rebel and G. W. Scheimer, Z. Phys. 262, 59 (1975).
[25]R. de Swiniarski, F. G. Resmini, D. L. Hendrie, and A. D. Bacher, Nucl. Phys. A261, 111 (1976).
[26]M. P. Fricke, E. E. Gross, and A. Zucker, Phys. Rev. 163, 1153 (1967).